Equilibrium Swelling and Universal Ratios in Dilute Polymer Solutions: *Exact* Brownian Dynamics Simulations for a Delta Function Excluded Volume Potential

K. Satheesh Kumar and J. Ravi Prakash*

Department of Chemical Engineering, Monash University, Clayton, Victoria 3800, Australia

Received March 9, 2003; Revised Manuscript Received August 3, 2003

ABSTRACT: A narrow Gaussian excluded volume potential, which tends to a δ-function repulsive potential in the limit of a width parameter d^* going to zero, has been used to examine the universal consequences of excluded volume interactions on the equilibrium and linear viscoelastic properties of dilute polymer solutions. Brownian dynamics simulations data, acquired for chains of finite length, have been extrapolated to the limit of infinite chain length to obtain model-independent predictions. The success of the method in predicting well-known aspects of static solution properties suggests that it can be used as a systematic means by which the influence of solvent quality on both equilibrium and nonequilibrium properties can be studied.

1. Introduction

There is a growing recognition of the importance of solvent quality in determining the rheological properties of dilute polymer solutions. Though there are relatively few systematic experimental investigations of the influence of solvent quality, nevertheless there is sufficient evidence to suggest that material functions, in both shear and extensional flows, are significantly different from each other in good and θ-solvents.[1−3] While the theoretical description of the influence of solvent quality on the equilibrium behavior of dilute polymer solutions has been a major area of research,[4−6] the description of its influence on nonequilibrium behavior is still in its infancy. Furthermore, most current nonequilibrium theories do not attempt to develop a unified framework that is also applicable at equilibrium, and the wealth of experience and insight that has been gained so far in the development of static theories is rarely used in the description of dynamic behavior. The central purpose of this paper is to introduce an approach for describing the influence of solvent quality far from equilibrium, which is consistent with our current understanding of its role in determining static solution behavior. As a first step toward establishing the usefulness of this methodology, we demonstrate its capability of reproducing some well-known universal static results. Even in the case of well-established results, the method is shown to provide some new and additional insights. Furthermore, as an example of the versatility of the approach, the influence of solvent quality on a universal ratio of linear viscoelastic properties is also obtained.

One of the most important results of the experimental investigation of the static behavior of dilute polymer solutions has been the discovery that various properties—both in θ-solvents and in good solvents—exhibit power law behavior when the molecular weight of the dissolved polymer is sufficiently large. It is perhaps less commonly known that even when the molecular weight is not very large, a type of scaling still persists, which enables the description of behavior with the help of a single parameter. An illustrative example is the behavior of the root-mean-square radius of gyration, R_g. Light scattering measurements indicate that, for molecules of sufficiently large molecular weight M, R_g obeys the power law $R_g = aM^\nu$, where the prefactor a depends on the particular polymer−solvent system but the exponent ν does not. In a θ-solvent, the universal exponent has a value, $\nu = 0.5$, while in a good solvent, $\nu = 0.592 \pm 0.003$.[7] A remarkable experimental observation is that, away from these large molecular weight asymptotic limits, the dependence of the mean size of the polymer molecule on both the temperature T of the solution and M can be combined into a single variable, $\hat{\tau}(T)\sqrt{M}$, where $\hat{\tau}(T)$ is a simple function of temperature, $\hat{\tau} = (1 - \theta/T)$, with θ denoting the θ-temperature. A vast amount of equilibrium data for a variety of polymer solvent systems reveals that, when the swelling α_g of a polymer molecule—defined as the ratio of the radius of gyration in a good solvent to the radius of gyration in a θ-solvent—is plotted as a function of $\hat{\tau}\sqrt{M}$ in a log−log plot, universal behavior can be obtained for all values of the molecular weight, M, and temperature, $T > \theta$, by merely shifting each polymer−solvent system horizontally by a suitable constant factor.[7−10]

The entire range of behavior exhibited by static solution properties has been successfully predicted by applying renormalization group (RG) methods.[4−6] In these theories, the macromolecule is frequently represented by a coarse-grained model, such as a bead−spring chain, consisting of N beads connected together by $(N - 1)$ Hookean springs (with a spring constant H). The presence of excluded volume interactions between parts of the polymer chain—which is believed to be the basic reason for the existence of degrees of solvent quality—is usually taken into account by assuming the existence of a Dirac delta function repulsive potential, which acts pairwise between the beads of the chain[11]

$$E(\mathbf{r}_{\nu\mu}) = \nu(T)k_B T\delta(\mathbf{r}_{\nu\mu}) \tag{1}$$

where $\nu(T)$ is the excluded volume parameter, k_B is Boltzmann's constant, and $\mathbf{r}_{\nu\mu}$ is the vector connecting beads ν and μ. In the limit $T \to \theta$, it can be shown that

* Corresponding author: e-mail ravi.jagadeeshan@eng.monash.edu.au.

10.1021/ma034296f CCC: $25.00
Published on Web 09/12/2003

v depends on T through the relation $v(T) = v_0\hat{\tau}(T)$, where v_0 is a constant.[11] If a length scale, $l = \sqrt{k_BT/H}$, and a nondimensional strength of excluded volume interactions, $z^* = v(2\pi l^2)^{-3/2}$, are defined, then both the temperature and the chain length dependence can be combined into the single nondimensional parameter $z = z^*\sqrt{N}$. Completely consistent with experimental observations (since $z \propto \hat{\tau}\sqrt{M}$), RG theories predict the existence of power laws in the limit $z \to 0$ (corresponding to a θ-solvent) and in the limit $z \to \infty$. The latter limit is usually termed the excluded volume limit; it corresponds to a good solvent at high temperature or to a good solvent in which the dissolved polymer molecules have a very large molecular weight. Significantly, renormalization group theories also predict the existence of scaling functions that depend only on the parameter z, which accurately describe the crossover behavior of all static properties between these two asymptotic limits, i.e., in the domain $0 < z < \infty$.[6]

Despite the success of RG theories, it must be borne in mind that they are approximate theories, dependent to some extent on the order of the original perturbation calculation on which they are based. *Exact* numerical results for the excluded volume problem can, on the other hand, be obtained by either Monte Carlo simulations of self-avoiding walks on lattices[12,13] or by off-lattice Monte Carlo simulations.[14] Since δ-functions cannot be used in numerical investigations, off-lattice Monte Carlo simulations are typically based on excluded volume potentials with a finite range of excluded volume interactions, such as the Lennard-Jones potential. An important point to be noted, however, is that the parameter z, which is the true measure of solvent quality, does not appear naturally when potentials like the Lennard-Jones potentials are used. Instead, simulation results are functions of the parameters that characterize the potential. It is possible, however, to infer the value of z from simulation results by carrying out a data shifting procedure similar to that used to bring experimental data onto a universal curve, i.e., data for various values of chain length N and various distances from the θ-temperature, can be brought to lie on a master curve.[14] The procedure is quite involved, and even the θ-temperature must first be estimated from simulations. Furthermore, Monte Carlo methods cannot be used to estimate rheological properties in general flow fields, and so it is not clear how this procedure can be extended to systematically examine the influence of solvent quality on nonequilibrium properties.

The self-similar character of polymer molecules, which is responsible for the universal behavior exhibited by polymer solutions at equilibrium, is also responsible for the universal behavior displayed away from equilibrium.[11] An important and fundamental challenge for molecular theories is to verify the existence of this universal behavior. The universal consequences of excluded volume effects away from equilibrium has been examined by Öttinger and co-workers[15,16] with the help of RG methods. Since these methods lead to approximate predictions, it is important to be able to assess their accuracy. Further, these papers were focused on predicting the universal behavior in the excluded volume limit, and crossover scaling functions for rheological properties were not reported.

In this paper, we introduce a procedure by which universal crossover scaling functions and asymptotic behavior in the excluded volume limit can be obtained for a δ-function excluded volume potential, both at equilibrium and away from it. There are two key aspects to this procedure. The first aspect is the use of the now well-established strategy for obtaining the universal predictions of a polymer model, namely, finding the model's predictions in the limit of infinite chain length. As is well-known, in this limit, the large number of degrees of freedom that are present make the large-scale predictions of the model, independent of model parameters. In the context of simulations, the infinite chain length limit is usually found by accumulating data for larger and larger values of N and then extrapolating the finite chain data to $N \to \infty$. The second key ingredient in our approach is the use of a narrow Gaussian potential to represent excluded volume interactions

$$E(\mathbf{r}_{\nu\mu}) = \left(\frac{z^*}{d^{*3}}\right)k_BT\exp\left\{-\frac{1}{2l^2}\frac{\mathbf{r}_{\nu\mu}^{\ 2}}{d^{*2}}\right\} \qquad (2)$$

where d^* is an nondimensional parameter that measures the range of excluded volume interaction. The narrow Gaussian potential, which was first suggested by Öttinger as a tool for examining excluded volume effects,[17] and subsequently used by Prakash and Öttinger in the context of a dumbbell model,[18] is a means of regularizing the δ-function potential since it reduces to the δ-potential in the limit of $d^* \to 0$.

At first sight, it appears that, apart from a length and time scale, the resultant theory would have three independent parameters, namely, z^*, N, and d^*, contrary to both experimental observations and RG theory results, which indicate that the only relevant variable is z. Interestingly, however—as has been established many years ago by the so-called two parameter theories[19]—as $N \to \infty$, the parameters z^* and N combine together to form the single variable, $z = z^*\sqrt{N}$. Furthermore, our previous investigations (which include an elementary renormalization group calculation[20] and asymptotic results obtained with an approximate version of the theory, namely, the so-called Gaussian approximation[21,22]) have shown that that the parameter d^* always appears in the theory as the rescaled variable $d^*/\sqrt{N}$. As a result, the choice of d^* becomes inconsequential in the limit $N \to \infty$. In the infinite chain limit, consequently, the only parameter in the theory is z. Indeed, universal predictions, both at equilibrium and in the linear viscoelastic limit,[20] and at finite shear rates in steady simple shear flow,[22] have been obtained earlier with the Gaussian approximation.

The central hypothesis therefore, behind the use of the narrow Gaussian potential, is that when data accumulated by carrying out *exact* Brownian dynamics simulations for chains of finite length are extrapolated to the infinite chain length limit, universal consequences of the presence of excluded volume interactions will be revealed, dependent solely on the value of the parameter z and independent of the value of d^*. Initial attempts to carry out this program were unsuccessful because of the large computational demands of Brownian dynamics simulations. In this paper, we show that a numerical solution can been obtained, and the computational difficulties encountered earlier can be overcome by adopting two novel solution strategies. As a result, a means has been obtained by which an *exact* numerical solution to the Edwards model, which is of fundamental importance to polymer physics, can be found, and the

influence of solvent quality, measured directly in terms of the parameter z, can be systematically examined.

The plan of the paper is as follows. In section 2, the governing stochastic differential equation and the equations governing the various equilibrium and linear viscoelastic properties are summarized. The solution procedure used in this work is outlined in section 3. In section 4, crossover scaling functions and universal properties in the excluded volume limit, found by extrapolating finite chain length results to the infinite chain length limit, are presented, and in section 5 the principal conclusions of this work are summarized.

2. Basic Equations

The internal configuration of a bead−spring chain suspended in a Newtonian solvent undergoing homogeneous flow, with its N beads located at positions $\boldsymbol{r}_\nu$, $\nu = 1, ..., N$, with respect to an arbitrarily chosen origin, can be specified by the $N - 1$ bead connector vectors, $\mathbf{Q}_k = \boldsymbol{r}_{k+1} - \boldsymbol{r}_k$, $k = 1, ..., N - 1$, connecting beads k and $k + 1$. Using the framework of polymer kinetic theory, and taking excluded volume interactions into account, a diffusion equation that governs the time evolution of the distribution of configurations of the bead−spring chain can be derived.[21] Since the diffusion equation is identically satisfied by Boltzmann's distribution in the absence of flow, it is equally applicable at equilibrium and away from it. Consequently, solving the diffusion equation would enable, at least in principle, the evaluation of averages of various configuration-dependent quantities in both regimes of behavior. Unfortunately, the diffusion equation is analytically intractable. However, *exact* numerical averages can be obtained by exploiting the mathematical equivalence of the diffusion equation in polymer configuration space and the stochastic differential equation for the polymer configuration. Since averages calculated from stochastic trajectories are identical to averages calculated from distribution functions, stochastic trajectories can be generated by numerically integrating the stochastic differential equation with the help of Brownian dynamics simulations.[17] This is the approach that has been adopted in the present work.

Introducing the following nondimensional variables

$$\mathbf{Q}_k^* = \frac{\mathbf{Q}_k}{l}; \quad t^* = \frac{t}{\lambda_H}; \quad \phi^* = \frac{\phi}{k_B T}; \quad \kappa^* = \lambda_H \kappa \tag{3}$$

where $\lambda_H = \zeta/4H$ is a time constant (with ζ representing the bead friction coefficient), $\kappa(t)$ is the traceless transpose of the velocity-gradient tensor for the homogeneous flow field, and ϕ is the total potential energy in the bead−spring chain due to the presence of Hookean springs and excluded volume effects

$$\phi = \frac{1}{2}H\sum_{i=1}^{N-1}\mathbf{Q}_i\cdot\mathbf{Q}_i + \frac{1}{2}\sum_{\substack{\nu,\mu=1\\ \nu\neq\mu}}^{N} E(\mathbf{r}_\nu - \mathbf{r}_\mu) \tag{4}$$

it can be shown that the stochastic differential equation for the bead-connector vectors has the form[21]

$$d\mathbf{Q}_j^* = \left[\kappa^*\cdot\mathbf{Q}_j^* - \frac{1}{4}\sum_{k=1}^{N-1}A_{jk}\frac{\partial\phi^*}{\partial\mathbf{Q}_k^*}\right]dt^* + \sqrt{\frac{1}{2}}\sum_{\nu-1}^{N}\bar{B}_{j\nu}\,d\mathbf{W}_\nu^* \tag{5}$$

Here, $\mathbf{W}_\nu^*$ is a Wiener process, whose $3N$-dimensional components satisfy

$$\langle W_{\nu,j}^*(t^*)\rangle = 0$$
$$\langle W_{\nu,j}^*(t^*)\, W_{\mu,k}(t^{*\prime})\rangle = \min(t^*,t^{*\prime})\delta_{jk}\delta_{\nu\mu} \tag{6}$$

for $j, k = 1, 2, 3$ and $\nu, \mu = 1, 2, 3, ..., N$. The quantity $\bar{B}_{k\nu}$ is an $(N - 1) \times N$ matrix defined by $\bar{B}_{k\nu} = \delta_{k+1,\nu} - \delta_{k\nu}$, with $\delta_{k\nu}$ denoting the Kronecker delta, and A_{jk} is the Rouse matrix

$$A_{jk} = \sum_{\nu=1}^{N}\bar{B}_{j\nu}\bar{B}_{k\nu} = \begin{cases} 2 & \text{for } |j-k| = 0 \\ -1 & \text{for } |j-k| = 1 \\ 0 & \text{otherwise} \end{cases} \tag{7}$$

It is important to note that hydrodynamic interactions between the different beads of the bead−spring chain have not been taken into account in the derivation of eq 5. Hydrodynamic interactions arise because of the propensity of the solvent to propagate disturbances in the velocity field caused by the motion of any particular bead to all the other beads in the chain, leading to a coupling of the motion of all the beads. While it is essential to incorporate hydrodynamic interactions in any molecular theory for the dynamic behavior of dilute polymer solutions, they do not alter any of the equilibrium properties, since the equilibrium configurational distribution function remains unchanged in the presence of hydrodynamic interactions. Advances made in the treatment of hydrodynamic interactions, in the context of polymer kinetic theory, have been reviewed recently by Prakash.[23] In this work, our primary focus is on introducing a novel treatment of excluded volume effects. Consequently, we have largely limited our discussion to the prediction of equilibrium properties. A universal ratio of linear viscoelastic properties has also been discussed here primarily to illustrate the advantages of using the present approach to treat excluded volume effects away from equilibrium. It is essential, however, to incorporate hydrodynamic interactions into the present theory, before a comparison can be made of the predicted value of the universal linear viscoelastic ratio with experimental results.

The stochastic differential equation for the well-known Rouse model—which was the first attempt to describe the rheological behavior of dilute polymer solutions in the context of bead−spring chains—is identical in form to eq 5.[17] The Rouse model, however, neglects excluded volume interactions. Consequently, the potential energy of the Rouse chain is determined entirely by the potential energy of the Hookean springs, and eq 4 therefore does not contain the second term on the right-hand side. The failure of the Rouse model to describe several of the observed features of polymer solution behavior has been attributed to its neglect of both excluded volume and hydrodynamic interactions.

On setting $\kappa = 0$, eq 5 describes the equilibrium trajectories of the bead-connector vectors. The same equation is consequently applicable both at equilibrium and away from it. In addition to equilibrium properties, as will be discussed in greater detail shortly, linear viscoelastic properties can also be obtained by carrying out equilibrium averages. As a result, all the properties of interest here are determined with the κ term set equal to zero in eq 5.

The equilibrium property that captures the influence of excluded volume effects most directly is the swelling of the radius of gyration, α_g. This quantity, as was pointed out earlier, is defined for experimental purposes as the ratio of the radius of gyration in a good solvent to the radius of gyration in a θ-solvent. In the present calculations, however, α_g is defined by

$$\alpha_g^2 = \left(\frac{R_g}{R_g^R}\right)^2 \tag{8}$$

where R_g^R is the radius of gyration predicted by the Rouse model[24]

$$R_g^R = l\sqrt{\frac{N^2-1}{2N}} \tag{9}$$

It is important to highlight the distinction between the experimental definition and the present definition of α_g because the Rouse model does not provide an entirely accurate description of the equilibrium properties of a θ-solution. As pointed out, for instance, in the detailed discussion by Schafer,[6] aspects of θ-solution behavior such as the corrections to random walk scaling due to the local stiffness of the chain, and the presence of three-body forces, are not taken into account in the Rouse model. Since the proper treatment of these effects within the context of the excluded volume problem is as yet a technically unresolved issue,[6] we have adopted the definition usually adopted in most molecular theories.

One can similarly define the swelling of the end-to-end vector α by

$$\alpha^2 = \frac{\langle \mathbf{r}^2\rangle}{\langle \mathbf{r}^2\rangle^R} \tag{10}$$

where $\langle \mathbf{r}^2\rangle$ is the mean-squared end-to-end vector in the presence of excluded volume interactions, and $\langle \mathbf{r}^2\rangle^R$ is the mean-square end-to-end vector of the Rouse model[24]

$$\langle \mathbf{r}^2\rangle^R = 3l^2(N-1) \tag{11}$$

Henceforth, a superscript or subscript "R" on any quantity will indicate a quantity defined or evaluated in the Rouse model, and angular brackets denote an average carried out with the equilibrium configurational distribution function.

The size of the polymer chain, represented by both R_g and $\sqrt{\langle \mathbf{r}^2\rangle}$, increases monotonically with increasing chain length. At equilibrium, for $M \gg 1$, both the quantities are known to exhibit power law dependencies on M, with identical exponents. The ratio

$$U_R = 6\frac{R_g^2}{\langle \mathbf{r}^2\rangle} \tag{12}$$

is consequently expected to become constant in the limit of large molecular weight. In the Rouse model, it is straightforward to see that U_R rapidly approaches a constant value of unit magnitude. It is of interest therefore to examine its behavior in the presence of excluded volume effects.

The linear viscoelastic properties considered here are the polymer contribution to the zero shear rate viscosity $\eta_{p,0}$ and the first normal stress difference coefficient $\Psi_{1,0}$. The second normal stress difference coefficient is identically zero since hydrodynamic interaction effects have not been taken into account.[24] Prakash[21] has shown earlier that, in the presence of excluded volume interactions, *exact* analytical expressions in terms of equilibrium averages can be obtained for both $\eta_{p,0}$ and $\Psi_{1,0}$ by developing a retarded motion expansion for the polymer contribution to the stress tensor. A detailed discussion of the development of the retarded motion expansion is given in ref 21. Here, we merely reproduce the final results

$$\eta_{p,0} = \frac{n_p\zeta}{6}\sum_{m,n=1}^{N-1} C_{mn}\langle \mathbf{Q}_m\cdot\mathbf{Q}_n\rangle \tag{13}$$

$$\Psi_{1,0} = \frac{n_p\zeta^2}{2k_BT}\sum_{m,n=1}^{N-1}\sum_{p,q=1}^{N-1} C_{mn}C_{pq}\langle Q_m^x Q_n^y Q_p^x Q_q^y\rangle \tag{14}$$

where Q_m^x, Q_m^y, and Q_m^z are the Cartesian components of the bead connector vector $\mathbf{Q}_m$, n_p is the number density of polymers, and C_{mn} is the Kramers matrix (which is inverse to the Rouse matrix), defined by

$$C_{mn} = \min(m, n) - \frac{mn}{N} \tag{15}$$

In the absence of excluded volume effects, eqs 13 and 14 can be shown to lead to the well-known analytical expressions for the zero shear rate viscosity and first normal stress difference coefficient in the Rouse model,

$$\eta_{p,0}^R = n_p\lambda_H k_B T\frac{N^2-1}{3} \tag{16}$$

$$\Psi_{1,0}^R = 2n_p\lambda_H^2 k_B T\left[\frac{(N^2-1)(2N^2+7)}{45}\right] \tag{17}$$

It is straightforward to see that in the Rouse model $\Psi_{1,0}^R$ scales as $(\eta_{p,0}^R)^2$ for large N. Analogously, in the presence of excluded volume effects, the ratio

$$U_{\Psi\eta} = \frac{n_p k_B T\Psi_{1,0}}{\eta_{p,0}^2} \tag{18}$$

is expected to become constant in the limit of large N. Renormalization group theories have shown that this is indeed true.[15] Here, we are interested in examining the behavior of $U_{\Psi\eta}$ as a function of the solvent quality z, both at finite z and in the limit $z \to \infty$.

Another important universal ratio that is frequently measured experimentally is $U_{\eta R}$, defined by[17]

$$U_{\eta R} = \frac{\eta_{p,0}}{n_p\eta_s(4\pi/3)R_g^3}$$

where η_s is the solvent viscosity. In the presence of excluded volume interactions (but not hydrodynamic interactions), the following expression relating the zero shear rate viscosity to the radius of gyration can be derived:[21]

$$\eta_{p,0} = \frac{n_p\zeta}{6}NR_g^2 \tag{19}$$

It is clear from this expression that the ratio $U_{\eta R}$ is not a universal ratio in the present model since it scales with N as $N^{1-\nu}$. It becomes a universal ratio only when hydrodynamic interaction effects are included in the model since this alters the scaling of $\eta_{p,0}$ with N. Consistent with the earlier discussion therefore, the prediction of $U_{\eta R}$ and its comparison with experiment require the extension of the present theory to include hydrodynamic interaction effects.

Before outlining the procedure by which eq 5 may be solved to obtain the *exact* values of the list of equilibrium and linear viscoelastic properties defined above, it is appropriate to discuss briefly the Gaussian approximation introduced earlier by Prakash.[21] The Gaussian approximation essentially consists of assuming that the nonequilibrium configurational distribution function remains Gaussian in the presence of excluded volume effects. A detailed discussion of the motivation and consequences of the Gaussian approximation may be found in the earlier works of Prakash.[21,22] In the present context, it is appropriate to note that *exact* expressions for the zero shear rate properties predicted by the Gaussian approximation can be derived by developing a codeformational memory integral expansion for the polymer contribution to the stress tensor.[21] Since the equations are rather cumbersome, and not by themselves very illuminating, they are presented in Appendix A for the sake of completeness. It suffices here to note that in the context of the Gaussian approximation the swelling of the end-to-end vector, and the zero shear rate viscosity and first normal stress difference coefficient, are given by eqs 31 and 32, respectively.

There are two reasons for discussing the Gaussian approximation in this work. First, since the Gaussian approximation was used earlier to predict universal properties[20,22] (motivated by its accurate prediction of finite chain properties in a limited range of parameter values), it is of interest to assess its accuracy in the infinite chain limit. Second, we shall see later that although the Gaussian approximation shares many of the universal features of the *exact* solution, it has a fundamental qualitative difference.

3. Simulation Strategies

The two basic goals of this work are to find the universal equilibrium and linear viscoelastic properties of a polymer solution in the excluded volume limit ($z \rightarrow \infty$) and in the crossover region between the θ-solution and excluded volume limits, i.e., for all $z > 0$.

Determining the universal properties in the excluded volume limit is relatively straightforward, since for any value of z^*, z ($= z^*\sqrt{N}$) $\rightarrow \infty$, as $N \rightarrow \infty$. We expect therefore that, when finite chain data, accumulated for constant values of z^* (which is equivalent to the temperature T being constant), are extrapolated to the infinite chain length limit, universal properties in the excluded volume limit will be obtained, independent of the particular choice of z^*.

A different procedure, however, is required for describing the crossover behavior. To determine the universal dependence of various properties on the parameter z, the value of z is kept constant at several predetermined magnitudes, and at each of these values, simulations are carried out for increasing values of N. The accumulated finite chain data, at each value of z, are subsequently extrapolated to the limit $N \rightarrow \infty$. The dependence on z, of the asymptotic values obtained in this manner, represents the universal crossover behavior. It is important to note that since during the extrapolation z has the same value at each value of N, it implies that $z^* \rightarrow 0$ (or, equivalently, $T \rightarrow \theta$) as $N \rightarrow \infty$. Clearly, therefore, this procedure leads to the prediction of universal crossover behavior for systems that are always close to the θ-temperature.

In both the schemes described above for obtaining universal predictions, the particular choice of d^* is irrelevant, since as mentioned earlier, though the value of d^* significantly influences results for finite chains, universal predictions are independent of the choice of d^*. Indeed, both these schemes have been used previously to obtain universal results in the Gaussian approximation.[20,22] In the constant z^* and the constant z numerical calculations, the value of d^* was held fixed at some arbitrarily small magnitude, and in each case, independence of the extrapolated results from the choice of d^* was clearly demonstrated.

The central aim of this work is to obtain *exact* universal predictions with the help of Brownian dynamics simulations rather than approximate predictions with the Gaussian approximation. The key obstacle to this goal has been the huge computational demand for solving eq 5, at large values of N. There are several reasons for the large computational requirement. The main culprit is of course the fact that the CPU time per time step scales with N as N^3. This arises because, for each value of the connector vector index j in eq 5, evaluation of the term $\sum_{k=1}^{N-1} A_{jk}(\partial\phi^*/\partial\mathbf{Q}_k^*)$ requires an N^2 operation. At present it seems difficult to change this scaling behavior without introducing some severe approximation to the model. On the other hand, there are other factors that contribute to the computational demand that can be circumvented by adopting a proper computational strategy. We discuss two such strategies that have been used in this work below.

The time step used to carry out the numerical integration is obviously an important factor determining the overall CPU time for the simulation. It has been found that, for comparable statistical error, a steeper narrow Gaussian potential necessitates a smaller time step. This has also been reported earlier in the case of the Lennard-Jones potential.[25−27] From the expression for ϕ in eq 4, it is straightforward to see that the narrow Gaussian potential appears in the drift term in eq 5 through the term $\partial E^*(\mathbf{r}_{\mu\nu}^*)/\partial\mathbf{Q}_k^*$. Using the expression for the narrow Gaussian potential in eq 2, one can show that

$$\frac{\partial E^*(\mathbf{r}_{\mu\nu}^*)}{\partial \mathbf{Q}_k^*} = \frac{z^*}{{d^*}^5} \exp\left[-\frac{\mathbf{r}_{\nu\mu}^{*\,2}}{2{d^*}^2}\right](B_{\mu k} - B_{\nu k})\,\mathbf{r}_{\nu\mu}^* \quad (20)$$

where the $N \times (N-1)$ matrix $B_{\nu k}$ is defined by $B_{\nu k} = (k/N) - \Theta(k-\nu)$, with $\Theta(k-\nu)$ denoting a Heaviside step function. The magnitude of this quantity has an extremum at $|\mathbf{r}_{\nu\mu}^*| = d^*$, which becomes larger as z^* increases or d^* becomes small, leading to the requirement of a smaller time step. It is possible, however, to develop a strategy to overcome this problem because we are only interested in the properties of the solution as $N \rightarrow \infty$.

As pointed out above, all numerical calculations in the Gaussian approximation were carried out at various small fixed values of d^*. This is because CPU time

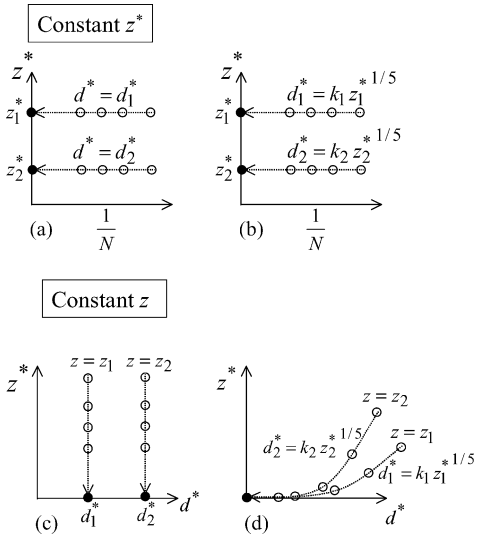

Figure 1. Illustration of the different simulation schemes used to obtain universal predictions. (a) and (b) correspond to runs at constant values of z^* and lead to universal predictions in the excluded volume limit; (c) and (d) correspond to runs at constant values of z and lead to universal crossover behavior predictions. Schemes (a) and (c) were used to obtain results in the Gaussian approximation, while (b) and (d) were adopted for Brownian dynamics simulations.

constraints are not so severe in that case. Consider, however, choosing the value of d^* such that

$$d^* = k(z^*)^{1/5} \tag{21}$$

where k is an arbitrary constant. This choice makes the magnitude of $\partial E^*(\mathbf{r}^*_{\mu\nu})/\partial \mathbf{Q}^*_k$ a weak function of z^*. As a result, the step size requirement becomes largely decoupled from the choice of d^* and z^*.

The various schemes discussed above are illustrated in Figure 1. Cases a and c correspond to procedures adopted previously in the Gaussian approximation. In scheme a, the open circles on a horizontal line correspond to calculations being performed at various values of N, while maintaining the values of z^* and d^* constant at some arbitrary values. Extrapolation of the finite chain data to the limit $N \to \infty$ leads to predictions in the excluded volume limit (denoted by the filled circles). These predictions are independent of the particular values chosen for d^* and z^*. The x-coordinate in Figure 1a,b is chosen to be $1/N$ merely to display the long chain limit. In scheme c, the open circles on a vertical line correspond to calculations performed at various values of N, with the parameters d^* and z kept constant. As mentioned earlier, since z is held constant, the asymptotic values obtained in the $N \to \infty$ limit correspond to $z^* \to 0$. Consequently, the arrows are in the direction of increasing N, and the filled circles, representing the asymptotic values, are displayed on the x-axis. Note that if $z_1 = z_2$, the asymptotic predictions are identical for both d_1^* and d_2^*.

Schemes b and d have been adopted while carrying out the Brownian dynamics simulations employed in this work. They correspond to using the expression 21 to find d^* for a given value of z^*, and as discussed above, this enables the use of relatively larger time steps. Case b is essentially identical to case a since the constants k_1 and k_2 are arbitrary. In case d, where constant z runs are performed to obtain the crossover behavior, using eq 21 implies that the $N \to \infty$ limit is reached along special trajectories in the (z^*, d^*) parameter space (as displayed schematically in Figure 1d). As in case c, the asymptotic limit corresponds to $z^* \to 0$. However, in this case it also corresponds to $d^* \to 0$. While asymptotic results are independent of the choice of d^* in scheme c, we shall show here that asymptotic results become independent of the value chosen for the constant k, when scheme d is adopted. Basically, the universal crossover behavior is independent of the trajectory in the (z^*, d^*) parameter space used to reach the long chain limit.

Another reason for the large computational demand arises from the need to keep the statistical errors in the finite chain data as small as possible in order to be able to obtain an accurate extrapolation of the data to the infinite chain length limit. If $X(\mathbf{Q}_1,\mathbf{Q}_2, ..., \mathbf{Q}_{N-1})$ is an arbitrary configuration-dependent quantity, with mean value $\langle X\rangle = \rho$ and with variance $(\langle X^2\rangle - \langle X\rangle^2) = \sigma^2$, and if it is desired to find ρ by Brownian dynamics simulations, then the standard procedure is to obtain N_T trajectories, or realizations, of X, and to carry out an ensemble average over these trajectories. The statistical error in the mean value is then given by $\sigma/\sqrt{N_T}$. Clearly, this error can be kept small by either keeping σ small or by using a large number of trajectories. The latter option is computationally expensive since reducing the error by an order of magnitude requires an increase in the number of trajectories by 2 orders of magnitude. On the other hand, a number of methods have been suggested for decreasing the variance σ, without simultaneously increasing the computational time significantly.[17]

In this work we have implemented a variance reduction procedure based on the method of control variates.[17] The first step in this scheme is to find a control random variable $X_c(\mathbf{Q}_1,\mathbf{Q}_2, ..., \mathbf{Q}_{N-1})$, whose mean value ρ_c is known exactly. Furthermore, the stochastic noise in X_c must be similar in magnitude to the noise in the variable of interest, namely, X. A new random variable $(X - X_c)$ is then defined, and N_T realizations of this variable are obtained by carrying out appropriate simulations. The mean value of interest can still be determined from these new simulations since

$$\rho = \langle X - X_c\rangle + \rho_c$$

Clearly, this estimate of the mean value has a statistical error $\sqrt{\mathrm{var}(X - X_c)/N_T}$, which is reduced relative to $\sigma/\sqrt{N_T}$, provided X and X_c are correlated. The key step is therefore the choice of the control variable X_c.

For the estimation of nonequilibrium viscoelastic properties at low shear rates, Wagner and Öttinger[28] suggested defining the control variable as the viscoelastic property calculated from a parallel equilibrium simulation, using the same starting configuration and same sequence of random numbers. In this case, $\rho_c = 0$, and as long as the nonequilibrium viscoelastic property and the viscoelastic property obtained from the parallel equilibrium simulation remain correlated, the reduction in variance is significant.

In this work, where all the properties of interest are obtained from an equilibrium simulation in the first place, the Wagner and Öttinger procedure cannot be used. Instead, we have defined the control variable X_c as the value of the quantity X obtained from the Rouse model, i.e., X_R. The mean value ρ_R is known analytically for all the properties of interest in this work. As pointed

out earlier, the only difference in the stochastic differential equation that governs the Rouse model from the stochastic differential equation, eq 5, that governs the present model, is that the term $\partial E^*(\mathbf{r}^*_{\mu\nu})/\partial \mathbf{Q}^*_k$ is missing in the drift term of the Rouse model.

The variance reduced simulation then consists of the following procedure. Both eq 5 and the Rouse stochastic differential equation are numerically integrated simultaneously, with the same starting configuration and same sequence of random numbers. For all the properties of interest X, N_T realizations of $(X - X_R)$ are then obtained. This does not increase the computational time significantly since the parallel Rouse simulation uses the same random numbers already generated for the main equilibrium simulation. The mean value $\langle X \rangle$ is then given by $\langle X \rangle = \langle X - X_R \rangle + \rho_R$, and the statistical error in this value is $\sqrt{\mathrm{var}(X - X_R)/N_T}$. For instance, the swelling of the end-to-end vector is obtained from

$$\alpha^2 = \frac{1}{3N-1}\langle(\mathbf{r}^{*2} - \mathbf{r}^{*2}_R)\rangle + 1$$

The use of this procedure has led to a significant reduction in the variance of all properties—typically by a factor of 3−5. This implies that a property calculated in the presence of excluded volume interactions and in the Rouse model have similar fluctuations about their mean values. As will be seen shortly, the reduction in variance that has been achieved has enabled an accurate extrapolation of finite chain data, even for fairly small chains.

Before presenting the main results of this work, we conclude this section with a few details of the simulations that were used to obtain them. Essentially, a second-order predictor−corrector algorithm originally proposed by Iniesta and Garcia de la Torre[29] was used to integrate eq 5. While the Iniesta and Garcia de la Torre algorithm also accounts for the presence of hydrodynamic interactions, the present algorithm is restricted to a treatment of excluded volume interactions alone. Explicit details of the algorithm, in the notation and context of the present work, can be found in ref 22. In a typical simulation, 10^5 trajectories were generated with a Gaussian initial distribution, and the integration was continued until a stationary state was attained (usually after a time equal to roughly 1.5 times the longest nondimensional Rouse relaxation time). Parallelization of the simulation was achieved by distributing the trajectories across the processors using message passing interface (MPI) clusters. This led to the wall time scaling with the number of processors used, and consequently, the present algorithm could be considered to belong to the class of embarrassingly parallel algorithms. A time-step extrapolation procedure enabled the simulations to be carried out at relatively large time steps. Typically, three different time steps $\Delta t^* = 1.0$, 0.6, and 0.5 were used, and the results were then extrapolated to zero time step using the subroutine TEXTRA developed by Öttinger.[17] These time steps were found to be adequate to obtain a reliable zero time-step extrapolation.

4. Universal Properties

Universal properties in the crossover region and in the excluded volume limit, obtained by using the different schemes described in Figure 1, are discussed in turn below. Before doing so, however, it is appropriate to list all the equations used to obtain them. *Exact* values of the swelling α^2, the zero shear rate viscosity $\eta_{p,0}$, and the zero shear rate first normal stress difference $\Psi_{1,0}$ are calculated using eqs 10, 13, and 14, respectively, with the equilibrium averages on the right-hand sides evaluated with the help of Brownian dynamics simulations. On the other hand, approximate values of α^2, $\eta_{p,0}$, and $\Psi_{1,0}$ are obtained with the help of the Gaussian approximation, using eqs 31 and 32. Since the radius of gyration is related to the zero shear rate viscosity through eq 19, the swelling α_g, defined by eq 8, can also be calculated simultaneously. Once these quantities are known, the universal ratios, U_R and $U_{\Psi\eta}$, can be evaluated using eqs 12 and 18.

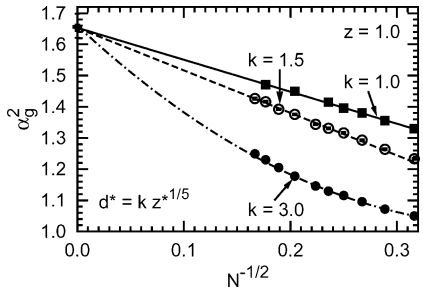

Figure 2. Square of the swelling of the radius of gyration, α_g^2 (see eq 8 for the definition), vs $1/\sqrt{N}$, at $z = 1$, for three vales of k. The symbols, with error bars, represent the simulation results, while the lines are least-squares curve fits to the data.

4.1. Crossover Behavior. As pointed out earlier, the procedure used here to obtain the universal crossover behavior leads to the descriptions of systems infinitesimally close to the θ-temperature. As a result, the crossover predictions of the present model are identical to the predictions of the continuum Edwards model.[6] In this context, it is worthwhile to note that rather than using the parameter z^* (or equivalently, ν) as a measure of the strength of excluded volume interactions, perturbative treatments of the Edwards model tend instead to use the cluster integral

$$\beta = \int \mathrm{d}\mathbf{r}_{\nu\mu}\left[\exp\left(-\frac{E(\mathbf{r}_{\nu\mu})}{k_B T}\right) - 1\right] \qquad (22)$$

We show in Appendix B that the two measures of excluded volume strength are identical in the continuum Edwards model but that it is more appropriate to use z^* in general Brownian dynamics simulations.

The independence of the predicted crossover behavior, from the trajectory in the (z^*, d^*) parameter space used to obtain it, is demonstrated graphically in Figure 2 for the swelling α_g^2. The parameter z is held constant at $z = 1$, while simulations are carried out for increasing values of N, up to $N = 36$. In each simulation, $z^* = z/\sqrt{N}$, while d^* is found from eq 21. Three sets of data, obtained for $k = 1$, 1.5, and 3, are plotted against $1/\sqrt{N}$ in Figure 2. The choice of $1/\sqrt{N}$ for the x-axis was motivated by two results obtained previously:[20] (i) the leading order corrections to the infinite chain length limit, of various material properties, is of order $1/\sqrt{N}$, and (ii) the parameter d^* always appears in the theory as $d^*/\sqrt{N}$. The convergence of all three curves in Figure 2, to a unique asymptotic limit, clearly demonstrates that in the limit $N \to \infty$ all material properties depend only on the variable z. Interestingly, for small values of k, the dependence of α_g^2 on $1/\sqrt{N}$ is almost

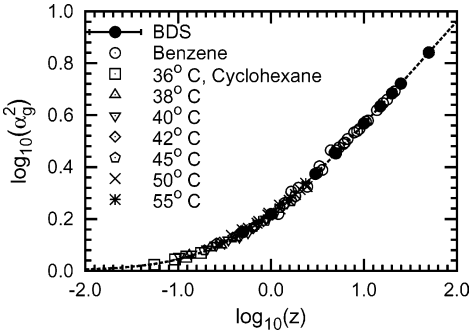

Figure 3. Asymptotic swelling of the radius of gyration vs the solvent quality. The filled circles are the predictions of Brownian dynamics simulations (BDS). Experimental data for polystyrene in the two solvents are from Miyaki and Fujita.[8] The dashed line represents a curve fit of the α_g^2 simulation data, using an equation of the form given in eq 23. The curve fit parameters are given in Table 1.

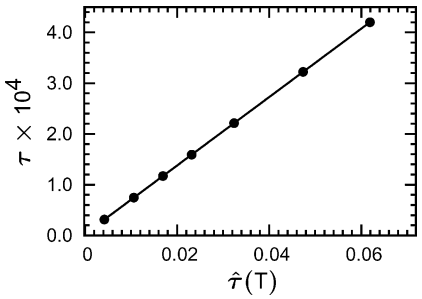

Figure 4. Dependence of $\tau = z/\sqrt{M}$ on the quantity $\hat{\tau}(T) = 1 - (\theta/T)$ for polystyrene in cyclohexane, where z is the theoretical solvent quality corresponding to the experimentally observed swelling at (T, M). Data are that of Miyaki and Fujita.[8]

linear, making the extrapolation more accurate. The values of α_g^2, obtained by carrying out this extrapolation procedure at various constant values of z, are displayed as the filled circles in Figure 3.

The experimental data of Miyaki and Fujita,[8] which are considered to be highly accurate measurements of the swelling of polystyrene in cyclohexane and benzene, obtained at various solvent temperatures and polymer molecular weights, can be plotted along with the theoretical data in Figure 3, by adopting the following procedure: (i) Several experimentally measured values of swelling, say $\alpha_g^\dagger$, are chosen, and the temperatures and molecular weights at which these values of swelling were observed (say $T^\dagger$ and $M^\dagger$) are noted. (ii) The values of z that correspond to these values of $\alpha_g^\dagger$ are then found from the theoretical simulation curve displayed in Figure 3. (iii) The parameter τ, defined by the expression $\tau = z/\sqrt{M^\dagger}$, is then calculated for each pair of values ($\alpha_g^\dagger$, z). (iv) The various values of τ obtained in this manner are plotted vs $\hat{\tau}(T^\dagger)$ (recall that $\hat{\tau}(T) = 1 - (\theta/T)$). The result of following this procedure for polystyrene in cyclohexane is shown in Figure 4, where the θ-temperature for this system, $\theta = 307.7$ K, has been used. The nearly perfect linear dependence of τ on $\hat{\tau}(T)$ indicates that the value of z that corresponds to any particular experimental pair (T, M) can be found from

$$z = \tau_0 \hat{\tau}(T) \sqrt{M}$$

where τ_0 is the slope of the τ vs $\hat{\tau}(T)$ line. Thus, as has been observed previously, a single material constant is sufficient to bring the entire set of experimental data onto a universal α_g^2 vs z curve. The remarkable agreement of the predicted equilibrium swelling with experimental data, similar to that found earlier by RG theory,[6] has been obtained here by using bead−spring chains with a maximum of just 36 beads.

Table 1. Coefficients in the Curve Fitting Function, Eq 23, Used To Fit the Data for α^2, α_g^2, and $\Psi_{1,0}/\Psi_{1,0}^R$, Obtained by Both Brownian Dynamics Simulations and the Gaussian Approximation[a]

	α_g^2	α^2	$\Psi_{1,0}/\Psi_{1,0}^R$
	Brownian Dynamics Simulation		
b	19.48 ± 1.28	14.24 ± 2.87	14.46 ± 0.57
c	14.92 ± 0.93	32.08 ± 2.27	15.73 ± 1.12
m	0.133913 ± 0.0006	0.134289 ± 0.0006	0.2536 ± 0.0015
ν	0.6004 ± 0.00045	0.6007 ± 0.00045	0.5951 ± 0.0011
	Gaussian Approximation Method		
b	10.30 ± 0.072	11.29 ± 0.26	8.63 ± 0.13
c	3.56 ± 0.056	4.18 ± 0.19	1.82 ± 0.12
m	0.213172 ± 0.00027	0.2164 ± 0.0008	0.4278 ± 0.002
ν	0.659879 ± 0.0002	0.6623 ± 0.0006	0.6604 ± 0.0007

[a] The scaling exponent ν is determined from the parameter m.

An expression commonly used to parametrize the results of RG calculations[6]

$$f(z) = (1 + az + bz^2 + cz^3)^m \qquad (23)$$

can be used to curve fit the values of α_g^2 obtained by Brownian dynamics simulations, displayed in Figure 3. Clearly, for $z \ll 1$, $f(z) = 1 + amz$. Perturbative treatments of the excluded volume problem have shown several years ago that, correct to first order in z, $\alpha_g^2 = 1 + 1.276z$.[19] Consequently, the values of the constants a, b, c, and m have been obtained here with the constraint that $am = 1.276$. The curve fit agrees closely with the simulation data, with the maximum difference between the data and the fit being less than 0.6%.

For $z \gg 1$, eq 23 implies that $\alpha_g^2 \sim z^{3m}$. Since $R_g \sim N^\nu$, $R_g^R \sim N^{0.5}$, and $z \sim N^{0.5}$, it follows that the exponent ν and the curve fit parameter m are related by the expression

$$\nu = \frac{1}{2} + \frac{3}{4}m \qquad (24)$$

The values of the curve fit parameters, and the value of ν obtained from eq 24, are given in first column (top half) of Table 1. As mentioned earlier, experimentally determined values of ν lie in the range $\nu = 0.592 \pm 0.003$.[7] The value $\nu = 0.588$ has been obtained by applying RG methods and is considered to be the most accurate estimate to date.[6] The present prediction of $\nu = 0.6004 \pm 0.0005$ is consequently about 2% greater than the value predicted by RG theory.

In Figure 5a, the crossover behavior of the swelling of the end-to-end vector α^2, predicted by Brownian dynamics simulations, is compared with the previously obtained crossover behavior predicted by the Gaussian approximation.[20] A similar comparison of the crossover behavior of the first normal stress difference coefficient ratio, $\Psi_{1,0}/\Psi_{1,0}^R$, is displayed in Figure 5b. The circles represent Brownian dynamics simulations results, while the squares represent predictions by the Gaussian approximation. The Gaussian approximation was shown previously by Prakash[21] to be exact to first order in z. It is not surprising therefore that the Gaussian approximation agrees with Brownian dynamics simula-

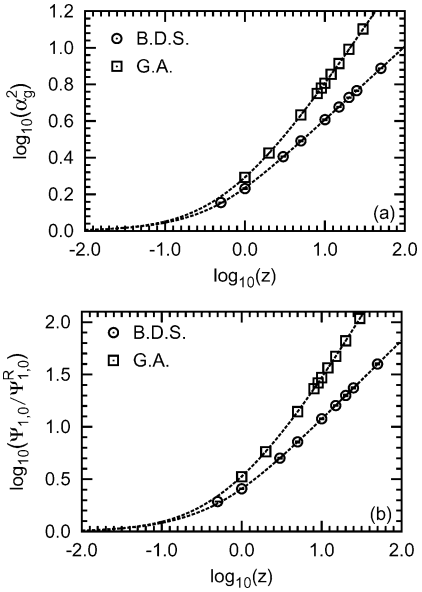

Figure 5. Comparison of the crossover behavior predicted by Brownian dynamics simulations with the predictions of the Gaussian approximation, reproduced from Prakash.[20] (a) Asymptotic swelling of the end-to-end vector and (b) asymptotic ratio of the zero shear rate first normal stress difference coefficient in the present model to that in the Rouse model. The open circles are Brownian dynamics simulation data, while the open squares are predictions of the Gaussian approximation. The dashed line is a curve fit using an equation of the form given in eq 23. Curve fit parameters are given in Table 1.

tions for $z \ll 1$. However, there is an increasing deviation between the two as z increases, indicating the non-Gaussian character of the distribution function in the presence of excluded volume effects.

Interestingly, the Brownian dynamics simulations data for both α^2 and $\Psi_{1,0}/\Psi_{1,0}^R$ can be curve fitted with functions of the form given in eq 23. In ref 20, the crossover predictions of the Gaussian approximation for α_g^2, α^2, and $\Psi_{1,0}/\Psi_{1,0}^R$ were curve-fitted by an expression similar to that in eq 23, but without the cubic term in z. Here, the data have been refitted with the cubic term included, for consistency with the curve fit used for the Brownian dynamics simulations results. The fact that both Brownian dynamics simulations and the Gaussian approximation must agree with first-order perturbation results imposes a constraint on the product am in these functions. In the case of α^2, the first-order perturbation result, $\alpha^2 = 1 + {}^4/_3 z$, is well-known,[19] while Prakash[21] has shown earlier that, correct to first order, $\Psi_{1,0}/\Psi_{1,0}^R = 1 + 2.41z$. The various curve fit parameter values used to fit the Brownian dynamics simulations and Gaussian approximation results are tabulated in Table 1. Since α^2 has the same scaling with molecular weight as α_g^2, the relation between the parameter m and exponent ν given in eq 24 is also valid for α^2. Making use of the fact that $\eta_{p,0}/\eta_{p,0}^R = \alpha_g^2$ and that $\Psi_{1,0} \sim (\eta_{p,0})^2$, one can show that the value of m for $\Psi_{1,0}/\Psi_{1,0}^R$ must be twice that for α_g^2. This expectation appears to be approximately satisfied by the values displayed in Table 1. Note that the exponent ν predicted by the Gaussian approximation is nearly 10% greater that the result obtained by *exact* Brownian dynamics simulations.

Although the scaling of R_g with chain length N obeys a power law only in the limit of long chains, one can

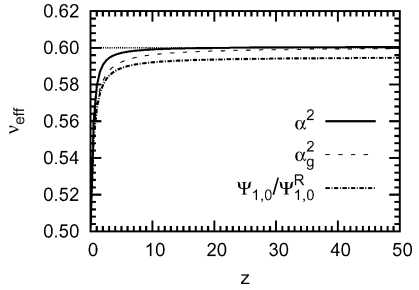

Figure 6. Effective exponent ν_{eff} obtained from the universal crossover behavior of α_g^2, α^2, and $\Psi_{1,0}/\Psi_{1,0}^R$, predicted by Brownian dynamics simulations.

make the ansatz that, at all values of chain length, $R_g \sim N^{\nu_{eff}}$, with ν_{eff} representing an effective exponent that approaches its critical value as $N \rightarrow \infty$. It is straightforward then to show that

$$\nu_{eff}(z) = \frac{1}{2} + \frac{1}{4}\frac{\partial \ln \alpha_g^2}{\partial \ln z} \tag{25}$$

The curve fitting function for α_g^2 can consequently be suitably differentiated to obtain the z dependence of the effective exponent ν_{eff}. In an entirely analogous manner, one can make an ansatz regarding the scaling behavior of both α^2 and $\Psi_{1,0}/\Psi_{1,0}^R$ with N. The dependence of ν_{eff} on z in each of these cases, for the *exact* results of Brownian dynamics simulations, is illustrated in Figure 6. While α^2 appears to approach the asymptotic scaling more rapidly than either α_g^2 or $\Psi_{1,0}/\Psi_{1,0}^R$, they all begin at the Rouse value, $\nu_{eff} = 0.5$, for $z = 0$, and approach $\nu_{eff} = 0.6$, as $z \rightarrow \infty$. It is worthwhile to note that ν_{eff} comes within 2% of its asymptotic value when z is in the range $5 \leq z \leq 10$. However, the final convergence occurs slowly. This has also been observed earlier in the case of RG theory predictions.[6]

The symbols in Figure 7a,b compare the crossover behavior of the two universal ratios U_R and $U_{\Psi\eta}$ predicted by Brownian dynamics simulations (filled circles) and the Gaussian approximation (filled squares). In the Rouse model, $U_R = 1$ and $U_{\Psi\eta} = 0.8$. It is clear from the figures that both the ratios begin at their respective Rouse values at $z = 0$ and decrease as z increases, approaching an asymptotic value for $z \rightarrow \infty$.

It has not been possible to obtain values of U_R and $U_{\Psi\eta}$ at even larger values of z because of the large computational demands of both Brownian dynamics simulations and the Gaussian approximation. For instance, to obtain an accurate extrapolation of finite chain data obtained by Brownian dynamics simulations, for values of $z > 50$, it is necessary to accumulate data for values of chain length much greater than $N = 40$. It is possible, however, to directly obtain the values of U_R and $U_{\Psi\eta}$ in the excluded volume limit, $z \rightarrow \infty$, as discussed below.

4.2. The Excluded Volume Limit. Using scheme a or b described earlier in the context of Figure 1, predictions in the excluded volume limit can be obtained, both in the case of Brownian dynamics simulations and for the Gaussian approximation. In Figure 8a,b, we discuss the results of following scheme b to obtain the universal ratios U_R and $U_{\Psi\eta}$ predicted by Brownian dynamics simulations. Three values of z^* were chosen, and d^* was determined from eq 21 with $k = 1$. Extrapolation of the finite chain data was

Table 2. Asymptotic Values of U_R and $U_{\Psi\eta}$ Predicted in the Excluded Volume Limit by Brownian Dynamics Simulations and the Gaussian Approximation for Different Values of z^*

z^*	U_R	$U_{\Psi\eta}$
	Brownian Dynamics Simulation	
0.24	0.9576 ± 0.0054	0.7705 ± 0.0093
0.28	0.9579 ± 0.0018	0.7699 ± 0.0027
0.35	0.9563 ± 0.0038	0.7700 ± 0.0031
	Gaussian Approximation	
0.30	0.9299 ± 0.00033	0.6064 ± 0.00012
0.35	0.9300 ± 0.00010	0.6069 ± 0.00008
0.40	0.9316 ± 0.00013	0.6059 ± 0.00035

carried out by assuming that the dependence of U_R and $U_{\Psi\eta}$ on N can be written as an expansion in powers of $(1/\sqrt{N})$

$$f(N) = A + \frac{B}{\sqrt{N}} + \frac{C}{N} + \frac{D}{N\sqrt{N}} + \frac{E}{N^2} + \ldots \quad (26)$$

As $N \to \infty$, the parameter A, which represents the infinite chain length limit, is expected to become independent of z^*. This is clearly demonstrated by the extrapolation curves for U_R and $U_{\Psi\eta}$ and by the asymptotic values for each value of z^*, reported in Table 2 (i.e., values of A, at different values of z^*, found by the extrapolation procedure). It was found necessary to include terms up to order $(1/N^2)$ in eq 26 in order to fit the data at small values of N. The data for $U_{\Psi\eta}$ have two distinctive features relative to that for U_R: (i) it is more scattered, and (ii) the values for different z^* appear closer to each other. The first of these features is because of the relatively larger variance associated with $\Psi_{1,0}$, while the second suggests that the coefficients B, C, etc., in the expansion (eq 26) for $U_{\Psi\eta}$ are weaker functions of z^*. The excluded volume limit value $U_R = 0.958 \pm 0.005$, predicted by the present Brownian dynamics simulations, is very close to the value $U_R = 0.959$ reported earlier by both RG theory and Monte Carlo simulations.[6] On the other hand, the value $U_{\Psi\eta} = 0.771 \pm 0.009$, predicted by the simulations, is significantly different from the value $U_{\Psi\eta} = 0.6288$ obtained earlier by RG theory based on refining a first-order perturbation expansion.[15] It is of interest to see whether a RG calculation based on a higher order perturbation theory would lead to better agreement with the present prediction. A possible alternative reason for this discrepancy is discussed later on.

The extrapolation scheme, described earlier in Figure 1a, has been used previously by Prakash[22] to obtain the Gaussian approximation's excluded volume limit predictions of the steady state viscosity and the first normal stress difference, at various finite values of the shear rate. On the other hand, though scheme c was used previously in ref 20 to obtain the Gaussian approximation's universal crossover behavior predictions of U_R and $U_{\Psi\eta}$, their values in the excluded volume limit were not obtained. To complete the comparison with Brownian dynamics simulations, the excluded volume limit values have been obtained here by applying scheme b to finite chain data generated by the Gaussian approximation. The values in Table 2 indicate that in the Gaussian approximation, as in the case of *exact* Brownian dynamics simulations, the excluded volume limit is independent of the particular choice of z^*. A comparison of the values predicted by the Gaussian approximation with the simulations results indicates the significant difference in the approximation's predictions from the *exact* values.

The data in Table 2 have been plotted as the various horizontal lines in Figure 7a,b along with the predictions of RG theories. It is immediately obvious that the crossover curves predicted by Brownian dynamics simulations do not tend to the asymptotic value predicted in the excluded volume limit. On the other hand, the crossover curves predicted by the Gaussian approximation do approach the predicted excluded volume limit value. Before we can discuss this intriguing behavior, and speculate as to its possible origin, we need to establish a number of results below.

Although the excluded volume limit is independent of z^*, there exists a special fixed point value, $z^* = z_f^*$, at which the finite chain data converges more rapidly to the excluded volume limit. This can be understood by considering eq 26. As mentioned earlier, while the parameter A is independent of z^*, the parameters B, C, etc., are functions of z^*. If $B = 0$ at some value of z^*, then the leading order correction changes from being of order $(1/\sqrt{N})$ to $(1/N)$, resulting in a more rapid approach to the long chain limit. While it is difficult to obtain the dependence of the leading order term on z^* analytically, we have attempted to determine it numerically from the predictions of Brownian dynamics simulations for the variables R_g and $\Psi_{1,0}$. Following Li et al.,[12] we can write

$$R_g^2 = N^{2\nu}\left(A_g + \frac{1}{\sqrt{N}} B_g\right)$$

$$\Psi_{1,0} = N^{4\nu+2}\left(A_\Psi + \frac{1}{\sqrt{N}} B_\Psi\right) \quad (27)$$

Simulation data for R_g and $\Psi_{1,0}$ as a function of N, obtained with $d^* = 1$, for various values of z^*, have been fitted with the expressions in eq 27, keeping the exponent ν fixed at the value $\nu = 0.6$. The dependence of B_g and B_Ψ on z^*, obtained in this manner, is displayed in Figure 9. The symbols denote the values of z^* at which the simulations were carried out. Both B_g and B_Ψ exhibit nearly linear behavior (with B_Ψ appearing to have a weaker dependence on z^*), crossing zero at a value of z^* in the range $0.26 \le z^* \le 0.29$. We shall see shortly that an alternative procedure can be used to find the fixed point, which also leads to a similar estimate of z_f^*. Prakash[22] has shown recently that the Gaussian approximation has a fixed point value $z_f^* \simeq 0.35$. As is evident from Table 2, the choice of values of z^* for the purpose of finding the universal ratios in the excluded volume limit has been motivated by the expectation that convergence occurs more rapidly in the vicinity of the fixed point. Indeed, the change in the sign of B_g, close to the fixed point, is clearly reflected in Figure 8a, where the asymptotic value of U_R is approached from above for $z^* = 0.24$, while it is approached from below for $z^* = 0.35$.

The basic premise of renormalization group theories is that the macroscopic properties of a polymer chain, in the excluded volume limit, should be independent of values chosen for model parameters at the level of the microstructure, such as the local length scale l (which is related to the mean size of a single connector vector in the bead−spring chain), the strength of excluded volume interaction between the beads, z^*, and the number of beads N. By repeatedly mapping the local

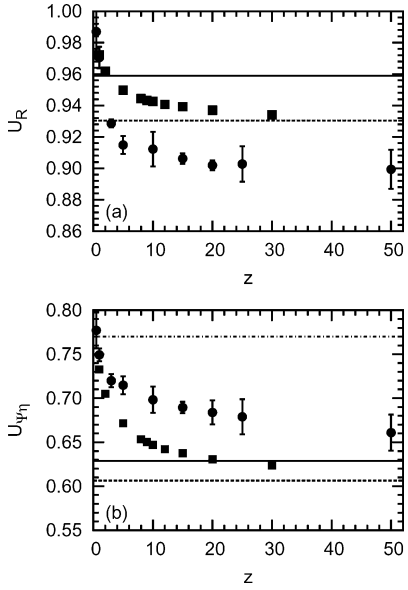

Figure 7. Crossover behavior of the universal ratios (a) U_R and (b) $U_{\Psi\eta}$. The filled circles are the predictions of Brownian dynamics simulations, while the filled squares are the results of the Gaussian approximation, reproduced from Prakash.[20] The various horizontal lines represent predictions in the excluded volume limit. The solid lines are predictions of RG theory,[6,15] the dashed lines are predictions of the Gaussian approximation, and the dot−dashed line represents the *exact* Brownian dynamics simulations prediction of $U_{\Psi\eta}$. In the case of U_R, the predictions of RG theory and simulations cannot be distinguished within the resolution of the figure.

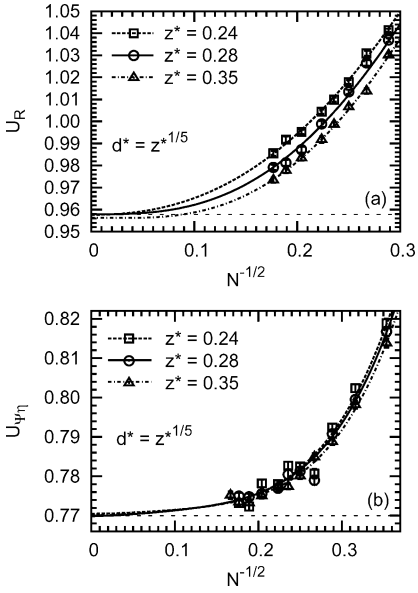

Figure 8. Universal ratios (a) U_R and (b) $U_{\Psi\eta}$ vs $1/\sqrt{N}$, at three different values of z^*. The curves are fits through the data using the functional form given in eq 26.

length scale l to larger and larger values, and N to smaller and smaller numbers of beads, while simultaneously maintaining macroscopic variable values unchanged, renormalization group theories show that the excluded volume parameter approaches a finite limiting value, termed the fixed point. As a result, at this fixed point, the properties of an infinitely long chain are shown to be captured by a model chain with a relatively small finite number of beads.[6] These arguments suggest that the existence of the fixed point is fundamentally linked to the existence of the excluded volume limit

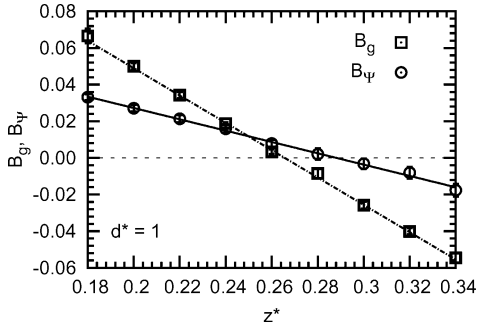

Figure 9. Coefficients B_g and B_Ψ, in the leading order correction term to the infinite chain length limit, for R_g^2 and $\Psi_{1,0}$, respectively (see eq 27 for the definition), vs the strength of excluded volume interaction z^*, at $d^* = 1$. Symbols denote the results of Brownian dynamics simulations, while the lines through the data are drawn to guide the eye.

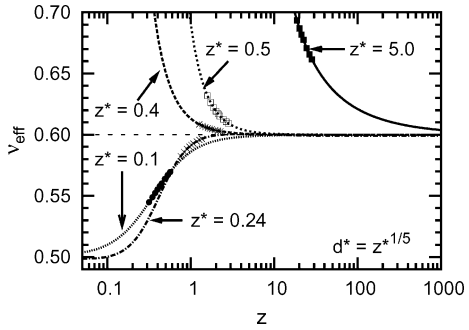

Figure 10. Exponent ν_{eff} in the expression $R_g \sim N^{\nu_{eff}}$ as a function of z. Symbols indicate the various values of N at which Brownian dynamics simulations have been carried out to obtain the z dependence of α_g^2. Values of ν_{eff} for $z^* > z_f^*$ (corresponding to the strong-coupling branch) and $z^* < z_f^*$ (corresponding to the weak-coupling branch) have been obtained by using the appropriate curve fitting expressions for the simulation data and eq 25.

(where the properties of the polymer solution become scale invariant and power law behavior is observed) and that an analogy between the present definition of the fixed point and the fixed point of RG theory can reasonably be drawn.

The fixed point of RG theory has also been shown by Schafer and co-workers[6,13] to be the value of z^* at which the solution to the excluded volume problem separates into two distinct branches. This is exemplified, for instance, by the behavior of the effective exponent ν_{eff} introduced earlier. Using both renormalization group methods and Monte Carlo simulations, Schafer and co-workers have shown that ν_{eff} approaches its critical value in the excluded volume limit, $\nu = 0.588$, on two distinct branches depending on whether $z^* < z_f^*$ (the weak-coupling branch) or $z^* > z_f^*$ (the strong-coupling branch). While the existence of a dual branched structure has only recently been elucidated, the various curves in Figure 10, for ν_{eff} as a function of z, show that Brownian dynamics simulations readily reveal the presence of this structure. The curves in Figure 10 have been obtained in the following manner: (i) α_g^2 vs z data, for $z^* < z_f^*$, were curve fitted with with $\alpha_g^2 = (1 + az + bz^2)^{2\nu-1}$; (ii) data for $z^* > z_f^*$ were curve fitted with $\alpha_g^2 = az^{4\nu-2}[1 - bz^{-|m|}(1 + c\,z^{-|1+m|})]$; and (iii) eq 25 was used to find ν_{eff} as a function of z. In both the curve-fitting expressions used for parametrizing the data (whose forms have been suggested earlier by Grassberger et al.[13]), the value of ν was set equal to 0.6.

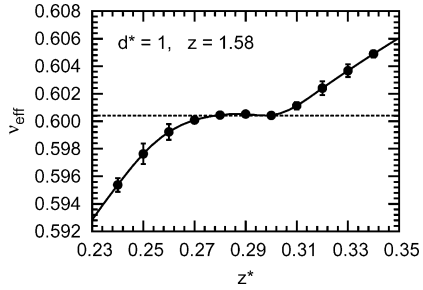

Figure 11. Effective exponent ν_{eff} as a function of the strength of excluded volume interactions z^*, predicted by Brownian dynamics simulations.

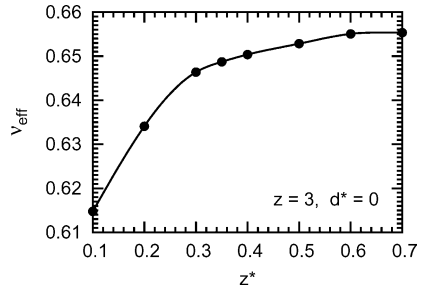

Figure 12. Effective exponent ν_{eff} as a function of the strength of excluded volume interactions z^*, predicted by the Gaussian approximation.

The distinctive dual branched structure of the solution can be exploited to develop a unique scheme by which both the fixed point and the critical exponent can be found. On the weak-coupling branch (strong-coupling branch), ν_{eff} first increases (decreases) rapidly before approaching the asymptotic value very gradually. We consequently expect a plot of ν_{eff} vs z^*, for constant values of d^* and z, to show a point of inflection at the fixed point. This is clearly seen in Figure 11, which describes the change in ν_{eff} as a function of z^*, for a range of values of z^* spanning the fixed point. To determine the displayed curve, eq 25 was used to find ν_{eff} by numerically differentiating ln α_g^2 vs ln z data at $z = 1.58$ (the data were obtained by carrying out simulations in the vicinity of $z = 1.58$, for various constant values of z^*, keeping $d^* = 1$). The figure suggests that the fixed point lies in the range $0.28 \leq z_f^* \leq 0.3$ and that the value of ν_{eff} in this range is 0.6004 $\pm$ 0.0002. This is expected to be close to the critical value, since asymptotic behavior is attained at relatively small values of N as $z^* \rightarrow z_f^*$.

It is of interest to examine whether the effective exponent predicted by the Gaussian approximation also exhibits a point of inflection at the fixed point. The curve displayed in Figure 12 was obtained by following the procedure outlined above for Brownian dynamics simulations results. Recall that the fixed point for the Gaussian approximation is $z_f^* \simeq 0.35$. Clearly, the curve does not have a point of inflection at 0.35. As can be seen from the values listed in Table 1, the exponent ν predicted by the Gaussian approximation is approximately equal to 0.66. Thus, at least for the value of z that was examined here, ν_{eff} always appears to lie below its critical value, suggesting that only the weak-coupling branch exists in the Gaussian approximation and that the dual branched structure of the *exact* solution is not captured. There is therefore a qualitative difference in the nature of the solution obtained by making the Gaussian approximation.

Having obtained the various results discussed so far in the present section, we return now to speculate on the possible origin of the intriguing results displayed earlier in Figure 7a,b, namely, the fact the crossover curves predicted by Brownian dynamics simulations do not asymptotically approach the values predicted in the excluded volume limit. As was pointed out earlier, the various crossover curves displayed in Figures 7 correspond to systems infinitesimally close to the θ-temperature. In the framework of the dual branched structure to the solution, the crossover curves might be considered to belong to a very special case of the weak-coupling branch, namely, to the case of $z^* \rightarrow 0$. On the other hand, the horizontal lines have all been obtained in the excluded volume limit, which is in a sense the ultimate reflection of the presence of excluded volume effects. It is perhaps the qualitatively different character of the two situations that is responsible for the fact that the crossover curves predicted by Brownian dynamics simulations do not tend in the limit of large z to the universal prediction obtained in the excluded volume limit. There is of course the unlikely possibility that the crossover curves have some structure beyond the largest value of z, namely $z = 50$, examined here. Interestingly, in the case of the Gaussian approximation, where the dual branched structure seems to be missing, the crossover curves do appear to asymptotically approach the results obtained in the excluded volume limit. It is also worthwhile to note that the crossover curve for $U_{\Psi\eta}$, predicted by Brownian dynamics simulations, appears to asymptotically approach the excluded volume limit value predicted by RG theory.[15] This suggests that perhaps the renormalization procedure pursued in ref 15 leads to universal predictions on the weak-coupling branch. It would also explain the large discrepancy between the excluded volume limit value of $U_{\Psi\eta}$ predicted by the present Brownian dynamics simulations and RG theory.

5. Conclusions

A novel procedure, applicable both at equilibrium and away from it, has been introduced in this work, by which universal crossover scaling functions and asymptotic behavior in the excluded volume limit can be obtained for a δ-function excluded volume potential. The usefulness of the procedure has been demonstrated by presenting results for equilibrium and linear viscoelastic properties.

The dependence of the swelling of the radius of gyration on solvent quality, predicted by adopting the present approach (Figure 3), has been shown to be in excellent agreement with the experimental observations of Miyaki and Fujita.[8]

Asymptotic values of the universal ratios U_R (eq 12) and $U_{\Psi\eta}$ (eq 18) have been obtained in the excluded volume limit. The predicted value, $U_R = 0.958 \pm 0.005$, is in excellent agreement with $U_R = 0.959$, predicted earlier by both RG theories and Monte Carlo simulations.[6] On the other hand, the predicted value $U_{\Psi\eta} = 0.771 \pm 0.009$ is significantly different from the prediction $U_{\Psi\eta} = 0.6288$ obtained earlier by a RG calculation based on refining a first-order perturbation expansion.[15]

Brownian dynamics simulations are shown to capture the dual branched structure of the solution, elucidated recently by Scäfer and co-workers[6,13] (Figure 10). This

distinctive structure has been exploited here to obtain an estimate of both the fixed point of the strength of excluded volume interactions and the critical exponent ν (Figure 11). It is an exciting prospect to see whether this dual branched structure persists into the nonequilibrium regime—an issue that is easily examinable within the framework introduced in this work.

The accuracy of the universal predictions of the Gaussian approximation[20,21] has been assessed by comparison with *exact* Brownian dynamics simulations (Figures 5, 7 and Tables 1, 2). The Gaussian approximation has been shown to be qualitatively different from the *exact* solution, since it appears not to capture its dual branched structure (Figure 12).

The asymptotic values of the *exact* crossover functions for U_R and $U_{\Psi\eta}$, in the limit of large z, are shown *not* to approach the universal predictions obtained in the excluded volume limit. On the other hand, the asymptotic predictions of the Gaussian approximation do tend to the values obtained in the excluded volume limit (Figure 7).

The overall agreement of the equilibrium and linear viscoelastic universal properties obtained here, with earlier results of Renormalization group theories, suggests that the narrow Gaussian potential, in conjunction with Brownian dynamics simulation, can serve as an excellent tool for the exploration of universal properties at equilibrium and away from it.

Acknowledgment. This project was supported by the Victorian Partnership for Advanced Computing (VPAC) Expertise Program Grant Scheme. We gratefully acknowledge both VPAC and the Australian Partnership for Advanced Computing for the use of their computational facilities.

Appendix A. Gaussian Approximation

The Gaussian approximation is centered on exploiting the assumption that the nonequilibrium distribution function is a Gaussian distribution. The most important consequence of this assumption is that the time evolution equation for the second moments of the distribution function becomes a closed expression for the second moments. Since we are only interested in equilibrium and linear viscoelastic properties in this work, the salient results in these limits are reproduced here.

The components f_{jk} of the equilibrium second moment tensor in the Gaussian approximation, $\langle \mathbf{Q}_j \mathbf{Q}_k \rangle = f_{jk}\mathbf{1}$, where $\mathbf{1}$ is the unit tensor, can be determined by numerically integrating the following system of ordinary differential equations[21]

$$\frac{\mathrm{d}}{\mathrm{d}t} f_{jk} = \frac{2k_BT}{\zeta} A_{jk} - \left(\frac{H}{\zeta}\right) \sum_{m=1}^{N-1} [f_{jm}\,(A_{mk} - z^*\Delta^{(0)}_{km}) + (A_{jm} - z^*\Delta^{(0)}_{jm})\, f_{mk}] \quad (28)$$

where

$$\Delta^{(0)}_{jm} = \sum_{\mu=1}^{N} \left[\frac{B_{j+1,m} - B_{\mu m}}{(d^{*2} + \hat{f}_{j+1,\mu})^{5/2}} - \frac{B_{jm} - B_{\mu m}}{(d^{*2} + \hat{f}_{j\mu})^{5/2}} \right] \quad (29)$$

Here, the $N \times (N-1)$ matrix $B_{\mu m}$ has been defined earlier below eq 20, and the quantities $\hat{f}_{\nu\mu}$ are defined by

$$\hat{f}_{\nu\mu} = \left(\frac{H}{k_BT}\right) \sum_{j,k=\min(\mu,\nu)}^{\max(\mu,\nu)-1} f_{jk} \quad (30)$$

The swelling of the end-to-end vector can then be shown to be given by

$$\alpha^2 = \left(\frac{H}{k_BT}\right)\frac{1}{N-1} \sum_{j,k=1}^{N-1} f_{jk} = \left(\frac{H}{k_BT}\right)\frac{1}{N-1}\, \hat{f}_{1N} \quad (31)$$

The two linear viscoelastic properties of interest here are the zero shear rate viscosity $\eta_{p,0}$ and zero shear rate first normal stress difference coefficient $\Psi_{1,0}$. As mentioned earlier, analytical expressions for both these quantities can be obtained by developing a codeformational memory integral expansion for the stress tensor[21]

$$\eta_{p,0} = 4\lambda_H \sum_{j,k=1}^{N-1} \sum_{m,n=1}^{N-1} \mathscr{H}_{jk} \bar{A}^{-1}_{jk,mn} f_{mn}$$

$$\Psi_{1,0} = 32\lambda_H{}^2 \sum_{j,k=1}^{N-1} \sum_{m,n=1}^{N-1} \sum_{r,s=1}^{N-1} \mathscr{H}_{jk} \bar{A}^{-1}_{jk,mn} \bar{A}^{-1}_{mn,rs} f_{rs} \quad (32)$$

The quantities on the right-hand sides of these expressions have lengthy definitions. They are presented in turn below. The quantity $\mathscr{H}_{jk}$ is defined by

$$\mathscr{H}_{jk} = n_p H \left(\delta_{jk} - \frac{1}{2} z^* \sum_{\substack{\mu,\nu=1 \\ \mu\neq\nu}}^{N} \frac{d^{*2}\theta(\nu,j,k,\mu)}{(d^{*2} + \hat{f}_{\nu\mu})^{7/2}} \right) \quad (33)$$

where the function $\theta(\mu,m,n,\nu)$ is unity if m and n lie between μ and ν and zero otherwise:

$$\theta(\mu,m,n,\nu) = \begin{cases} 1 & \text{if } \mu \le m,\ n < \nu \text{ or } \nu \le m,\ n < \mu \\ 0 & \text{otherwise} \end{cases} \quad (34)$$

The $(N-1)^2 \times (N-1)^2$ matrix $\bar{A}_{jk,mn}$ is defined by

$$\bar{A}_{jk,mn} = (A_{jm}\delta_{kn} + \delta_{jm}A_{kn}) - z^*(\Delta^{(0)}_{jm}\delta_{kn} + \delta_{jm}\Delta^{(0)}_{kn}) + z^*\left(\frac{H}{k_BT}\right)\sum_{p=1}^{N-1} [f_{jp}\Delta^{(1)}_{kp,mn} + \Delta^{(1)}_{jp,mn} f_{pk}] \quad (35)$$

where

$$\Delta^{(1)}_{jp,mn} = \sum_{\mu=1}^{N} \left[\frac{(B_{j+1,p} - B_{\mu p})\theta(\mu,m,n,j+1)}{(d^{*2} + \hat{f}_{j+1,\mu})^{7/2}} - \frac{(B_{jp} - B_{\mu p})\theta(\mu,m,n,j)}{(d^{*2} + \hat{f}_{j\mu})^{7/2}} \right] \quad (36)$$

Appendix B. The Cluster Integral

In this appendix, we examine the suitability of using the cluster integral to represent the strength of excluded volume interactions, when the narrow Gaussian poten-

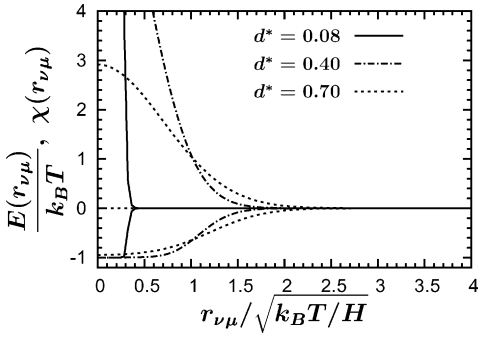

Figure 13. Nondimensional narrow Gaussian repulsive potential energy $E(\mathbf{r}_{\nu\mu})/k_BT$ and the function $\chi(\mathbf{r}_{\nu\mu})$ vs the nondimensional magnitude of the interbead vector $r_{\nu\mu}/\sqrt{k_BT/H}$, for various values of the range of interaction d^*. Curves above x-axis represent $E(\mathbf{r}_{\nu\mu})/k_BT$, while curves below the x-axis represent $\chi(\mathbf{r}_{\nu\mu})$.

tial is used to model the interactions. If we define the function

$$\chi(\mathbf{r}_{\nu\mu}) = \exp\left(-\frac{E(\mathbf{r}_{\nu\mu})}{k_BT}\right) - 1 \tag{37}$$

then the cluster integral can be written as

$$\beta = \int d\mathbf{r}_{\nu\mu}\, \chi(\mathbf{r}_{\nu\mu}) \tag{38}$$

It is straightforward to show, for a hard-core repulsive potential defined by

$$E(\mathbf{r}_{\nu\mu}) = \begin{cases} \infty & \text{for } r_{\nu\mu} < \sigma \\ 0 & \text{for } r_{\nu\mu} > \sigma \end{cases} \tag{39}$$

(where $r_{\nu\mu}$ is the magnitude of the interbead vector, $r_{\nu\mu} = |\mathbf{r}_{\nu\mu}|$ and σ is the radius of the hard core), that eq 37 leads to

$$\chi(\mathbf{r}_{\nu\mu}) = \begin{cases} -1 & \text{for } r_{\nu\mu} < \sigma \\ 0 & \text{for } r_{\nu\mu} > \sigma \end{cases} \tag{40}$$

As a result

$$\beta = \int_0^\sigma dr_{\nu\mu}\, 4\pi r^2(-1) = -\frac{4}{3}\pi\sigma^3 \tag{41}$$

The cluster integral is consequently related to the volume of the hard core and clearly becomes smaller as the radius of the hard core is reduced. If $E(\mathbf{r}_{\nu\mu})$ is given by the narrow Gaussian potential (eq 2), then in the limit $d^* \to 0$ (as can be seen graphically in Figure 13) the function $\chi(\mathbf{r}_{\nu\mu})$ is nonzero and equal to -1 only at the origin and goes to zero everywhere else. Consequently, the cluster integral β is identically zero in the limit $d^* \to 0$. Clearly, this result is related to the result derived above for the cluster integral of a hard-core potential, in the limit of the radius of the hard core $\sigma \to 0$. In the context of the narrow Gaussian potential, using a cluster integral to characterize the strength of interactions would therefore not lead to the Edwards model in the limit $d^* \to 0$.

The cluster integral is frequently used in perturbative treatments of the Edwards model because well-established cluster function methods can be used to carry out expansions in powers of β. As mentioned earlier, the continuum Edwards model corresponds to the limit $T \to T_\theta$ or $v \to 0$. Consequently, it is meaningful to carry out a perturbation expansion of $\exp(-E(\mathbf{r}_{\nu\mu})/k_BT)$ for small values of v:

$$\exp\left(-\frac{E(\mathbf{r}_{\nu\mu})}{k_BT}\right) = 1 - \frac{E(\mathbf{r}_{\nu\mu})}{k_BT} + \frac{1}{2}\left(\frac{E(\mathbf{r}_{\nu\mu})}{k_BT}\right)^2 + \ldots \tag{42}$$

If all higher order terms are neglected, it follows from eq 37 that $\chi(\mathbf{r}_{\nu\mu}) = -E(r_{\nu\mu})/k_BT$. On substituting the repulsive potential of the Edwards model (eq 1) for $E(\mathbf{r}_{\nu\mu})$ and evaluating the cluster integral given by eq 38, one can see that

$$\beta = -\int d\mathbf{r}_{\nu\mu} v\delta(\mathbf{r}_{\nu\mu}) = -v \tag{43}$$

Thus, in the limit of small v, and to first order, the excluded volume parameter is indeed identical to the cluster integral.

A famous result of the classical statistical mechanical theory of fluids[30] is the fact that, for an imperfect gas, the second virial coefficient, $B_2(T)$, is simply related to the cluster integral, i.e., $B_2(T) = -\beta/2$. Doi and Edwards[11] point out that if the total interaction energy in the chain is written (in the continuous chain limit) as

$$U_1 = \frac{1}{2}vk_BT\int_0^N d\nu \int_0^N d\mu\, \delta(\mathbf{r}_\nu - \mathbf{r}_\mu) = \frac{1}{2}vk_BT\int d\mathbf{r}\, c(\mathbf{r})^2 \tag{44}$$

where $c(\mathbf{r}) = \int_0^N d\mathbf{r}\, \delta(\mathbf{r} - \mathbf{r}_\nu)$ is the local concentration of segments, then this expression can be regarded as the first term in the expansion of the free energy with respect to the local concentration, and consequently, v can be regarded as being proportional to the virial coefficient between the segments. On the basis of this result, it is common to draw an analogy with the result recalled above for an imperfect gas and to suggest that v must be given by the cluster integral

$$v = \int d\mathbf{r}_{\nu\mu}\left[1 - \exp\left(-\frac{E(\mathbf{r}_{\nu\mu})}{k_BT}\right)\right] \tag{45}$$

This is not rigorously true, and is in fact only true in the limit of small v, as we have seen above.

In conclusion, it is appropriate to use v (or z^*) as the parameter that characterizes the strength of excluded volume interactions when carrying out *exact* Brownian dynamics simulations, and it can be seen to be representing a measure of the contribution of excluded volume interactions to the total potential energy of the chain.

References and Notes

(1) Noda, I.; Yamada, Y.; Nagasawa, M. *J. Phys. Chem.* **1968**, *72*, 2890−2898.
(2) Solomon, M. J.; Muller, S. J. *J. Rheol.* **1996**, *40*, 837−856.
(3) Sridhar, T.; Nguyen, D. A.; Fuller, G. G. *J. Non-Newtonian Fluid Mech.* **2000**, *90*, 299−315.
(4) Freed, K. F. *Renormalization Group Theory of Macromolecules*; Wiley: New York, 1987.
(5) des Cloizeaux, J.; Jannink, G. *Polymers in Solution, Their Modeling and Structure;* Oxford Science Publishers: New York, 1990.
(6) Schäfer, L. *Excluded Volume Effects in Polymer Solutions;* Springer-Verlag: Berlin, 1999.
(7) Hayward, R. C.; Graessley, W. W. *Macromolecules* **1999**, *32*, 3502−3509.
(8) Miyaki, Y.; Fujita, H. *Macromolecules* **1981**, *14*, 742−746.

(9) Vidakovic, P.; Rondelez, F. *Macromolecules* **1985**, *18*, 700−708.
(10) Bercea, M.; Ioan, C.; Ioan, S.; Simionescu, B. C.; Simionescu, C. I. *Prog. Polym. Sci.* **1999**, *24*, 379−424.
(11) Doi, M.; Edwards, S. F. *The Theory of Polymer Dynamics*; Oxford University Press: Oxford, 1986.
(12) Li, B.; Madras, N.; Sokal, A. D. *J. Stat. Phys.* **1995**, *80*, 661.
(13) Grassberger, P.; Sutter, P.; Schäfer, L. *J. Phys. A: Math. Gen.* **1997**, *30*, 7039−7056.
(14) Graessley, W. W.; Hayward, R. C.; Grest, G. S. *Macromolecules* **1999**, *32*, 3510−3517.
(15) Öttinger, H. C. *Phys. Rev. A* **1989**, *40*, 2664−2671.
(16) Zylka, W.; Öttinger, H. C. *Macromolecules* **1991**, *24*, 484−494.
(17) Öttinger, H. C. *Stochastic Processes in Polymeric Fluids*; Springer-Verlag: Berlin, 1996.
(18) Prakash, J. R.; Öttinger, H. C. *Macromolecules* **1999**, *32*, 2028−2043.
(19) Yamakawa, H. *Modern Theory of Polymer Solutions*; Harper and Row: New York, 1971.
(20) Prakash, J. R. *Chem. Eng. Sci.* **2001**, *56*, 5555−5564.
(21) Prakash, J. R. *Macromolecules* **2001**, *34*, 3396−3411.
(22) Prakash, J. R. *J. Rheol.* **2002**, *46*, 1353−1380.
(23) Prakash, J. R. The Kinetic Theory of Dilute Solutions of Flexible Polymers: Hydrodynamic Interaction. In *Advances in the Flow and Rheology of Non-Newtonian Fluids*; Siginer, D. A., Kee, D. D, Chhabra, R. P., Eds.; Rheology Series; Elsevier Science: Amsterdam, 1999.
(24) Bird, R. B.; Curtiss, C. F.; Armstrong, R. C.; Hassager, O. *Dynamics of Polymeric Liquids*, 2nd ed.; John Wiley: New York, 1987; Vol. 2.
(25) Rey, A.; Freire, J. J.; Garcia de la Torre, J. *Polymer* **1992**, *33*, 3477−3482.
(26) Andrews, N. C.; Doufas, A. K.; McHugh, A. J. *Macromolecules* **1998**, *31*, 3104−3108.
(27) Cifre, J. G. H.; Garcia de la Torre, J. *J. Rheol.* **1999**, *43*, 339−358.
(28) Wagner, N. J.; Öttinger, H. C. *J. Rheol.* **1997**, *41*, 757−768.
(29) Iniesta, A.; Garcia de la Torre, J. *J. Chem. Phys.* **1990**, *92*, 2015−2018.
(30) Reichl, L. E. *A Modern Course in Statistical Physics*; Edward Arnold: London, 1991.

MA034296F